Water Research 103 (2016) 1–9

Contents lists available at ScienceDirect

Water Research

journal homepage: www.elsevier.com/locate/watres

Reductive transformation of tetrabromobisphenol A by sulfidated nano zerovalent iron

Dan Li [a, d], Zhe Mao [a, d], Yin Zhong [a, *], Weilin Huang [c], Yundang Wu [a, b, d], Ping'an Peng [a]

[a] State Key Laboratory of Organic Geochemistry, Guangzhou Institute of Geochemistry, Chinese Academy of Sciences, Wushan, Guangzhou 510640, China
[b] Guangdong Key Laboratory of Agricultural Environment Pollution Integrated Control, Guangdong Institute of Eco-Environmental and Soil Sciences, Guangzhou, China
[c] Department of Environmental Sciences Rutgers, The State University of New Jersey, 14 College Farm Road, New Brunswick, NJ 08901, USA
[d] University of Chinese Academy of Sciences, Beijing 100049, China

ARTICLE INFO

Article history:
Received 17 January 2016
Received in revised form
18 June 2016
Accepted 2 July 2016
Available online 5 July 2016

Keywords:
TBBPA
S-nZVI
Sulfidation
Transformation pattern
Reusability
Aging

ABSTRACT

Recent studies showed that sulfidated nano zerovalent iron (S-nZVI) is a better alternative to non-sulfidated nano zerovalent iron (NS-nZVI) commonly used for contaminated site remediation. However, its reactivity with different halogenated pollutants such as tetrabromobisphenol A (TBBPA) remains unclear. In this study, we explored the reductive transformation of TBBPA by S-nZVI and compared it with that by NS-nZVI. The results showed that over 90% of the initial TBBPA (20 mg L^{-1}) was transformed by S-nZVI within 24 h of reaction, which was 1.65 times as high as that for NS-nZVI. The TBBPA transformation by S-nZVI was well described by a pseudo-first-order kinetic model, whilst that by NS-nZVI was well fitted by a three-parameter single exponential decay model. After 11 weeks of aging, S-nZVI was still able to transform up to 56% of the initial TBBPA within 24 h of reaction; by contrast, the two-week aged NS-nZVI lost more than 95% of its original capacity to transform TBBPA. Moreover, S-nZVI showed only an approximately 20% decrease in its capacity to transform TBBPA in the seventh cycle, while NS-nZVI was no longer able to transform TBBPA in the fourth cycle. XPS analysis suggested the formation of FeS layer on S-nZVI surface and electrochemical analysis revealed an elevated electron transfer capacity of S-nZVI, which were likely responsible for the superior performances of S-nZVI in TBBPA transformation. While the transformation rate of TBBPA by S-nZVI decreased with increasing initial concentration of TBBPA, it showed an increasing trend with increasing S/Fe ratio and initial concentration of S-nZVI. The study indicated that S-nZVI has the potential to be a promising alternative to NS-nZVI for remediation of TBBPA-contaminated aquatic environments.

1. Introduction

Tetrabromobisphenol A (TBBPA) is the most abundantly applied brominated flame retardant (BFR) with an annually worldwide demand over 170, 000 tons in 2004 (Covaci et al., 2009). Approximately 90% of TBBPA is used in printed circuit boards as a reactive BFR and the remaining 10% is used in plastic polymers as an additive BFR (Alaee et al., 2003). The widespread use of TBBPA and its incomplete removal from waste printed circuit boards and plastic waste during waste treatment have already led to the large-scale release of TBBPA into the environment. Recent reports documented that the levels of TBBPA in leachates from industrial landfills were up to 620 ng L^{-1} (Osako et al., 2004), whereas those of TBBPA in effluents from sewage treatment works could be as high as 85 ng L^{-1} (Morris et al., 2004). Despite its hydrophobic nature, TBBPA can be transported and accumulated in aquatic environments. Indeed, residues of TBBPA have been widely detected in a variety of water, sediment and aquatic organism samples (e.g., Morris et al., 2004; Harrad et al., 2009; He et al., 2013). Remarkably, a maximum concentration up to 9.75 mg kg^{-1} was found for the TBBPA residues in river sediments from England (Morris et al., 2004). TBBPA is known as a thyroid hormone agonist as well as an estrogen (Kitamura et al., 2002; Decherf et al., 2010). It was thought to cause lethal effects on aquatic organisms like fish and algae even at low concentrations (Darnerud, 2003). Therefore, it is of great importance to develop effective methods to remove TBBPA from contaminated aquatic environments.

* Corresponding author.
E-mail address: zhongyin@gig.ac.cn (Y. Zhong).

http://dx.doi.org/10.1016/j.watres.2016.07.003
0043-1354/

In the last decade, nanoscale zerovalent iron (nZVI) has been recognized as a promising option for dealing with soils, groundwater and sediments contaminated by chlorinated organic compounds due to its high reactivity and low cost (O'Carroll et al., 2013; Mukherjee et al., 2016). More recently, there has been evidence that nZVI also has the potential to remediate TBBPA-contaminated environmental matrices (Lin et al., 2012). Note, however, that iron can react with water and cause precipitation of iron oxide or hydroxide on the surface of nZVI, which can dramatically reduce the reactivity of nZVI and thereby its efficiency in contaminant (e.g., TBBPA) removal (Guan et al., 2015). Several types of strategies have been devised to improve the reactivity of nZVI to target contaminants (such as TBBPA). Firstly, nZVI-based bimetals (e.g., Fe/Pd and Fe/Ni) were synthesized and demonstrated in the lab to have a greater reactivity towards TBBPA compared to nZVI (Huang et al., 2013; Li et al., 2016a). Secondly, the combination of either nZVI or nZVI-based bimetals with physical approaches (e.g., ultrasound assistance and microwave radiation) was found to be able to enhance the transformation rate of TBBPA (Luo et al., 2010, 2011). Thirdly, the addition of bentonite has proven to be a useful option for accelerating the transformation of TBBPA by nZVI (Yan et al., 2013). Unfortunately, these alternative strategies also seem to suffer from some inherent limitations: (1) the short lifetime of nZVI-based bimetals and the potential toxicity of noble metals released from these bimetals are of considerable concern (Guan et al., 2015), (2) physical approaches are generally hard to implement in the field for reasons related to the high energy costs (Ince et al., 2001; Remya and Lin, 2011), and (3) the synergistic effects of bentonite and nZVI would be weak if the bentonite was not closely contacted with nZVI (Guan et al., 2015).

Recently, the potential roles of sulfidated nanoscale zerovalent iron (S-nZVI) in remediation of sites contaminated by chlorinated organic compounds, has gained increasing attention, because there is evidence that it can assist in maximizing the benefits of nZVI-based approaches and helping to overcome their limitations. First of all, S-nZVI was found to have a higher reactivity towards certain contaminants than non-sulfidated nanoscale zerovalent iron (NS-nZVI). For example, Rajajayavel and Ghoshal (2015) reported that the degradation rate constant of trichloroethylene (TCE) by S-nZVI was approximately 40 times greater than that of NS-nZVI. Similar results were also observed by Kim et al. (2011, 2013). Secondly, the reactivity of S-nZVI with contaminants tends to be more stable than that of NS-nZVI. As demonstrated by Kim et al. (2013), the effects of groundwater solutes on TCE removal capacity of S-nZVI were less pronounced than their effects on that of nZVI. Thirdly, unlike other nZVI-based materials that are synthesized through a series of complex procedures, S-nZVI can be produced simply via a single-step synthesis (Kim et al., 2011; Rajajayavel and Ghoshal, 2015). Indeed, S-nZVI may occur naturally in the environment through microbially-assisted sulfidation of NS-nZVI (Rickard, 1995; Watson et al., 2000). Fourthly, sulfidation is expected to reduce the toxicity of NS-nZVI as little toxicity was observed for other sulfidated nanoparticles (Reinsch et al., 2012; Levard et al., 2013). Lastly, such a readily available material is cost-effective compared to other nZVI-based bimetals consisting noble metals. It is therefore interesting to explore the potential use of S-nZVI as an attractive candidate for remediation of sites contaminated by brominated organic compounds (e.g., TBBPA). However, little laboratory research has been done to address such an intriguing topic.

In this study, the performance of S-nZVI in mediating TBBPA transformation was investigated for the first time and compared with that of NS-nZVI under a set of uniform conditions. The comparison was focused on not only the transformation patterns (including rate, dynamic, transformation product and pathway) but also the longevity and reusability as these factors are very important for the potential use of nZVI-based nanoparticles in remediation of TBBPA contamination. Further, the effects of S/Fe molar ratio, S-nZVI dosage and initial TBBPA concentration on the performance of S-nZVI in TBBPA transformation were examined. Unlike the previous studies in which a water/cosolvent mixture containing 50% of cosolvent (v/v) was used to prepare reaction solutions for TBBPA transformation by nZVI-based materials (e.g., Huang et al., 2013; Li et al., 2016a), here a water/cosolvent mixture with only 2% of cosolvent was used as the reaction solution in order to decrease the effect of cosolvent on TBBPA transformation. Therefore, the results of this study can help not only improving our understanding of the reactivity of S-nZVI with TBBPA and but also developing S-nZVI-based remedial options that may be applicable to various aquatic environments contaminated by TBBPA.

2. Materials and methods

2.1. Chemical reagents

TBBPA standard (97%), bisphenol A (BPA) standard (99%) and ferrous chloride ($FeCl_2$, ultra dry, 99.99%) were purchased from Alfa Aesar (Ward Hill, USA). Standards of tri-BBPA, di-BBPA and mono-BBPA were obtained from Dr. Yu's laboratory of Guangzhou Institute of Geochemistry, Chinese Academy of Sciences (Wang et al., 2016). Sodium borohydride ($NaBH_4$, 98%) and dithionite ($Na_2S_2O_4$, 98%) were purchased from Fisher Scientific (Pittsburgh, USA). Concentrated HCl (37%, w/w) was guaranteed reagent of Guangzhou Chemical Reagents Factory (Guangzhou, China). HPLC-grade methanol was obtained from Merck (Darmstadt, Germany). The deionized water (18.2 MΩ cm) was autoclaved at 121 °C for 20 min, and then deoxygenated with high purity nitrogen (99.999%) for 30 min prior to use for preparation of all solutions.

2.2. Preparation and characterization of NS-nZVI and S-nZVI

NS-nZVI was prepared in an anaerobic glovebox (Super 1220/750, Mikrouna Co. Ltd., Shanghai, China) filled with high purity nitrogen (99.999%) according to the method reported by Üzüm et al. (2008) with minor modifications. In brief, 60 mL of $FeCl_2$ solution (0.2 M) was reduced with 180 mL of $NaBH_4$ (0.3 M) solution using a pear-shaped funnel equipped with a magnetic stirring bar. After reduction, the resulting precipitate was collected by centrifugation, washed with deionized water five times, followed by washing once with deoxygenated ethanol. Subsequently, the precipitate was dried with high purity nitrogen (99.999%) and stored in sealed vials in an anaerobic glovebox until use.

S-nZVI was synthesized as follows. 60 mL of $FeCl_2$ solution (0.2 M) was added into 180 mL of a mixed solution of $NaBH_4$ (0.3 M) and $Na_2S_2O_4$ (0.017 M) which prescribed sulfidation of nZVI at an S/Fe molar ratio of 0.51. The resulting precipitate was collected and treated in a similar manner for NS-nZVI. In order to examine the effect of S/Fe molar ratio on the performance of S-nZVI in transformation of TBBPA, two extra types of S-nZVI particles at S/Fe molar ratios of 0.12 and 0.24 were synthesized with a similar procedure. Unless otherwise stated, the S-nZVI used in subsequent experiments was referred to that synthesized at an S/Fe molar ratio of 0.51.

The Brunauer-Emmett-Teller (BET) specific surface areas of NS-nZVI and S-nZVI particles were measured by the N_2 physisorption on an ASAP 2020 instrument (Micromeritics, Atlanta, USA). As expected, the BET specific surface area (14.3 $m^2\ g^{-1}$, Table S1 in Supporting Information) of the NS-nZVI synthesized in this study was comparable to that (14.2 $m^2\ g^{-1}$) of the NS-nZVI synthesized by Üzüm et al. (2008). Additionally, it was found that the BET specific surface areas of the three types of S-nZVI particles were larger than

that of the NS-nZVI (Table S1), which was consistent with the finding of Kim et al. (2011). The surface compositions of the synthetic NS-nZVI and S-nZVI were examined by an ESCALAB-250 X-ray photoelectron spectrometer (XPS; Thermo VG Scientific, West Sussex, UK) according to the method described by Rajajayavel and Ghoshal (2015).

2.3. Batch experiments

TBBPA transformation batch experiments were conducted in 150 mL screw capped glass bottles with PTFE-lined silicone septa containing 100 mL of aqueous suspension of 2.3 g L^{-1} NS-nZVI or S-nZVI and 20 mg L^{-1} TBBPA in an anaerobic glovebox. TBBPA stock solution was prepared in methanol. The reaction was initiated by adding an appropriate amount of TBBPA stock solution into the suspensions, respectively. The content of methanol in the reaction solution (methanol/water mixture) was 2% (v/v). The reaction bottles were placed on a magnetic stirrer at 300 rpm in dark at 25 °C. Two mL aliquots were taken from each reaction suspension and added into 5 mL glass bottles capped with open top closures with PTFE-lined silicone septa for analysis of TBBPA and its transformation products at different sampling times (i.e., 1, 2, 4, 6, 9, 12 and 24 h after the initiation of the reactions). Twenty μL of 5 M HCl was injected into each of the 2-mL suspensions to dissolve the solids and facilitate the release of TBBPA and its transformation products from the solids to the solution phase. Subsequently, 2 mL of methanol was added into each of the resulting solutions. After being mixed thoroughly, 1-mL aliquot was collected from the solutions for the analysis of TBBPA and its transformation products with the method described below. All experiments were conducted in duplicate and the relative standard deviations of all data were below 5%.

To further compare the performances of NS-nZVI and S-nZVI on transformation of TBBPA, the effects of aging and the reusability of the two types of particles were examined. Specifically, the performances of the NS-nZVI and S-nZVI particles aged in deionized water for 0, 1, 2, 4, 7 and 11 weeks were investigated in 5-mL glass bottles under the same experiment conditions as described above, respectively. A smaller reaction system was used since we focused on the 24-h performance rather than the transformation rate during the 24-h period. To investigate their reusability, fresh NS-nZVI and S-nZVI particles were used to react with TBPPA for 7 repetitive cycles; each had freshly introduced TBPPA and was run under the same reaction conditions as for the experiments designed for quantifying the effects of aging. In each cycle, 1-mL aliquots of reaction solution were collected from individual bottles after 24 h of reaction for the quantification of TBBPA, and the remaining was centrifuged at 6000 rpm for 5 min. After centrifugation, the supernatant was descanted and the solid phase was used in next cycle of reaction.

To evaluate the effects of initial concentrations of both TBBPA and S-nZVI on TBBPA transformation, additional batch experiments were performed in 150-mL glass bottles under experiment conditions as described above. The initial concentrations of TBBPA (5, 10 and 20 mg L^{-1}) tested here were comparable to those reported in anoxic sediments (Morris et al., 2004), while those of S-nZVI (0.6, 1.2 and 2.3 mg L^{-1}) fell within the concentration range used in other prior studies (Rajajayavel and Ghoshal, 2015; Su et al., 2015).

2.4. Chemical analysis

The transformation products of TBBPA were identified on an Agilent 1200 series liquid chromatography coupled to an Agilent 6410 electrospray triple quadrupole mass spectrometer (LC-MS) with an Agilent ZORBAX Eclipse Plus C18 reversed-phase column (250 × 4.6 mm, 5 μm particle size; Agilent, Santa Clara, USA). The mobile phase was a mixture of methanol/water (v/v, 8/2) and the flow rate was 1 mL min^{-1}. The sample injection volume was 20 μL. The LC-MS analysis procedures including mobile phases, flow rates, and sample injection volumes were identical with those of HPLC-UV analysis described below. The mass spectrometric analysis was performed using electrospray ionization (ESI) in negative ion mode with a scan range from 45 to 700 amu. Four transformation products including tri-BBPA, di-BBPA, mono-BBPA and BPA were identified by comparing their retention time and mass spectra with those of their respective corresponding standards. No other debrominated product was detected with the LC-MS method and the two isomers of di-BBPA could not be distinguished by the HPLC method.

The concentrations of TBBPA and its transformation products (i.e., tri-BBPA, di-BBPA, mono-BBPA and BPA) were determined by Shimadzu LC-20A HPLC-UV system (Shimadzu, Kyoto, Japan). The HPLC-UV analytical procedures including column, mobile phases, flow rates, and sample injection volumes were identical to those of LC-MS analysis described above. The wavelength was set at 210 nm and the peaks of TBBPA and its transformation products on the chromatograms of HPLC-UV had the same retention time to those of LC-MS (Fig. S1). The quantification of TBBPA and BPA were performed using their respective external standards. The quantities of the tri-BBPA, di-BBPA, and mono-BBPA synthesized in Dr. Yu's lab were very limited due to the sophisticated procedures for synthesis and purification of these chemicals. Thus, no external standards of these intermediate products were used for their quantification with the HPLC-UV method. Alternatively, the concentrations of tri-BBPA, di-BBPA, and mono-BBPA in aqueous phase were estimated from their HPLC peak areas based on the standard curves of TBBPA and BPA on a molar basis with compensation for the number of bromine atoms (Huang et al., 2013; Li et al., 2016a). The summed molar concentrations of TBBPA, tri-BBPA, di-BBPA, mono-BBPA and BPA of individual samples ranged from 96% to 105% of the initial TBBPA concentrations in respective batch experiments, which was consistent with the fact (as mentioned above) that no other TBBPA transformation products were detected by the LC-MS.

For quality assurance and quality control (QA/QC), the HPLC-UV was calibrated routinely with calibration standards and the relative percent difference among different analyses was less than 10%. The linear standard curves of TBBPA and its transformation products were obtained with the range from 0.50 to 12.0 mg L^{-1}, and the linear regression analysis of standard curves of TBBPA and its products showed good linearity ($R^2 > 0.997$). Reagent blanks (reaction solution of water/methanol mixture; v/v, 98/2), S-nZVI or NS-nZVI blanks (reaction solution with S-nZVI or NS-nZVI addition), TBBPA controls (reaction solution spiked with TBBPA), and spiked control samples (S-nZVI or NS-nZVI blanks spiked with TBBPA) were processed in duplicate for each batch experiment. While TBBPA was not detected in the blank samples, the recoveries of TBBPA for the TBBPA controls and spiked control samples were 100.6± 0.8%, 99.8± 0.4% and 98.7± 1.1%, respectively. The limits of detection (LODs) and limits of quantification (LOQs) were calculated for every single analyte, considering a signal-to-noise ratio of 3 and 10, respectively. The LODs for TBBPA, tri-BBPA, di-BBPA and mono-BBPA and BPA were 0.017, 0.018, 0.020, 0.022 and 0.024 mg L^{-1}, respectively. The LOQs for TBBPA, tri-BBPA, di-BBPA and mono-BBPA and BPA were 0.055, 0.060, 0.065, 0.072 and 0.080 mg L^{-1}, respectively.

2.5. Electrochemical analysis

The electrochemical properties of NS-nZVI and S-nZVI were characterized with the cyclic voltammetry (CV) and

electrochemical impedance spectroscopy (EIS) performed on a CHI660D electrochemical workstation (CH Instrument Co., Shanghai, China) with a conventional three-electrode cell. The electrolyte solutions were deoxygenated by purging nitrogen (99.999%) for 20 min before use, and nitrogen condition in the cell was maintained throughout the experiments. Prior to modification, the bare glassy carbon electrode (GCE, 3 mm diameter) was polished with 0.1 and 0.05 μm alumina powder, respectively. After the polishing process, the bare GCE was washed three times in an ultrasonic bath with ultra-pure water, twice with a mixture of ultra-pure water and ethanol (v/v, 1:1) and once with a mixture of ultra-pure water and concentrated HNO_3 (v/v, 1:1), respectively. The bare GCE was cycled in 1 M H_2SO_4 until a stable voltammogram was obtained. The well prepared bare GCE was then modified with the film of either NS-nZVI or S-nZVI in an anaerobic glovebox, respectively. A mixture containing 0.2 mol L^{-1} PBS and 20 mg L^{-1} TBBPA was used for determining CVs and EIS of the modified GCEs. While CVs were recorded in a potential range between −1.0 and 0.3 V at a scan rate of 0.05 V s^{-1} for 6 cycles, EIS measurements of the cells were conducted at the amplitude of 0.005 V and the frequency ranging from 10^5 to 0.01 Hz.

3. Results and discussion

3.1. Overall performances of S-nZVI and NS-nZVI in TBBPA transformation

As shown in Fig. 1, after 24 h of reaction, 91% of the initial TBBPA (20 mg L^{-1}) was transformed by S-nZVI, compared favorably to a 55% reduction by NS-nZVI, indicating a 36% increase in the capacity for TBBPA transformation by S-nZVI. Such an elevated capacity could be attributed to the formation of an FeS layer on the nZVI surface. The XPS analysis showed S^{2-}, S_2^{2-} and Fe(II)-S were present on the surface of S-nZVI (Table 1, Text S1 and Fig. S2), suggesting that iron sulfides (i.e., FeS and FeS_2) may be formed on the S-nZVI surface. By contrast, S^{2-}, S_2^{2-} and Fe(II)-S were not detected on the NS-nZVI surface; instead, iron oxide and hydroxide (i.e., Fe_3O_4 and FeO(OH); Table 1, Text S1 and Fig. S2) were main species found on NS-nZVI. Meanwhile, Table 1 and Fig. S2 showed that Fe(0) was present on the surface of NS-nZVI, but not on S-nZVI. It is intuitive that the formation of FeS on nZVI surface may have enhanced the efficiency of electron conduction between nZVI and the contaminants due to the excellent electrical conductivity of iron sulfides (Kim et al., 2011; Rajajayavel and Ghoshal, 2015). This hypothesis was supported strongly by our electrochemical analysis as S-nZVI had a higher electron transfer capacity than NS-nZVI. As shown in the CV cycle profiles (Fig. 2A), the redox peaks of S-nZVI-modified GCE had a higher current density but a smaller pear-to-peak separation (0.346 V *vs* 0.401 V) as compared to those of NS-nZVI-modified GCE, indicating a better electrochemical reversibility of S-nZVI (Zheng et al., 2009). Furthermore, the typical Nyquist plots (Fig. 2B) showed that the S-nZVI-modified GCE had a smaller semicircle diameter but lower Z″ values at high frequency than the NS-nZVI-modified GCE, suggested that S-nZVI had a greater overall rate of electron transfer than NS-nZVI (Turcio-Ortega et al., 2012). The observed elevated capacity of TBBPA transformation by S-nZVI was also likely because iron sulfide surface on S-nZVI had greater hydrophobicity than iron oxide surface of NS-nZVI as more hydrophobic binding sites favor stronger interactions with hydrophobic TBBPA (Vaughan and Ridout, 1971; Kim et al., 2011). Moreover, the elevated transformation capacity by S-nZVI could also have resulted from its lowered aggregation tendency due to deposition of FeS on nZVI surface (Su et al., 2015), which was consistent with greater BET SSA of S-nZVI than NS-nZVI (Table S1). It is important to note, however, that our recent study (Li et al., 2016b) demonstrated no reaction of chemically synthesized pure FeS phase with TBBPA under similar experiment conditions of this study. Thus, iron sulfides on the S-nZVI surface are less likely to have directly participated in the reaction between TBBPA and S-nZVI.

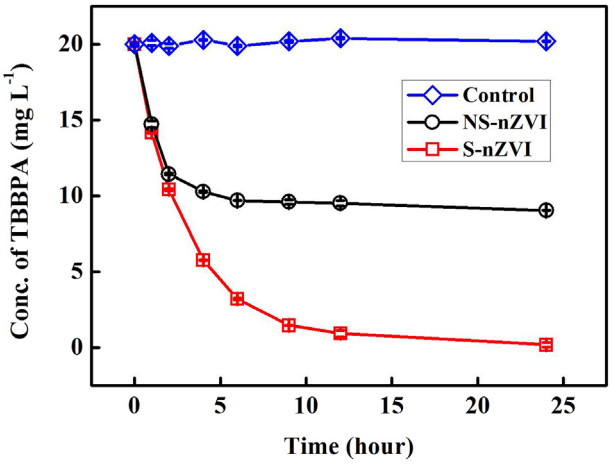

Fig. 1. The overall performances of S-nZVI and NS-nZVI in TBBPA transformation. Concentrations of TBBPA remaining in the reaction solutions at different time points are shown (means ± standard errors).

3.2. Products and pathways of TBBPA transformation by S-nZVI and NS-nZVI

Four TBBPA transformation products (i.e., tri-BBPA, di-BBPA, mono-BBPA and BPA) were found in the S-nZVI system after a 24-h reaction (Text S2 and Fig. 3). By contrast, BPA was not detectable in the NS-nZVI system (Text S2 and Fig. 3D), wherein the three incompletely debrominated products of TBBPA were detected (Fig. 3A–C). Note also that mono-BBPA concentration in the NS-nZVI system was barely above its detection limit after reaction for 24 h, compared to a concentration level of 7.5 mg L^{-1} (Fig. 3C) measured for the S-nZVI system. It is likely that BPA may be eventually formed in the NS-nZVI system if the reaction lasted for longer time periods as indicated in Lin et al. (2012), but its concentration would be much lower than in the S-nZVI system. Nevertheless, rapid formation of BPA in the S-nZVI system should be considered as an advantage over the NS-nZVI system since BPA is less toxic and readily degradable than brominated BPA (McCormick et al., 2010; Chang et al., 2012; Yang and Chan, 2015). On the basis of the transformation products identified in this study, the transformation pathways of TBBPA in the S-nZVI and NS-nZVI systems were proposed (Text S3 and Fig. S4). In brief, TBBPA may undergo a sequential debromination pathway to form less brominated products or even non-brominated product. During each step, only one bromine atom was likely replaced by a hydrogen atom. Indeed, similar pathways have also been proposed previously for the transformation of TBBPA by other iron-based nanoparticles such as nZVI, Ag/Fe, Ni/Fe and Fe/SiO_2 (Luo et al., 2010; Lin et al., 2012; Zhang et al., 2012; Li et al., 2016a).

3.3. Kinetics of TBBPA transformation by S-nZVI and NS-nZVI

The time-dependent TBBPA concentration profile over 24-h in the NS-nZVI system could be adequately fit to a three-parameter single exponential decay model proposed by Lin et al. (2012) (Text S4 and Fig. S5). By contrast, the TBBPA concentration profile measured for the S-nZVI system could be well described by a four-

Table 1
XPS binding energies (BE) of Fe($2p_{3/2}$), S(2p), and O(1s) and the relative abundances of Fe, S and O species on NS-nZVI and S-nZVI (S/Fe ratio = 0.51) surfaces.

Sample	Species		BE/(eV)[a]	Relative abundance (area, %)	Ref.
nZVI	Fe($2p_{3/2}$)	Fe(0)	706.7	13.56	Bae et al., 2016
		Fe(II)-O	709.3	34.64	Bae et al., 2016
		Fe_3O_4 and FeO(OH)	711.5	24.32	Shahwan et al., 2011
	O(1s)	O_2^-	529.9	41.91	Pirlot et al., 2001
		OH^-	531.1	32.43	Pirlot et al., 2001
		H_2O	532.0	25.66	Pirlot et al., 2001
S-nZVI	Fe($2p_{3/2}$)	Fe(II)-S	707.3	7.17	Mullet et al., 2002
		Fe(II)-O	710.0	37.45	Pirlot et al., 2001
		Fe_3O_4 and FeO(OH)	712.4	27.28	Jeong et al., 2010
	O(1s)	O^{2-}	530.0	17.47	Mullet et al., 2002
		OH^-	531.2	48.88	Mullet et al., 2002
		H_2O	532.1	33.66	Harvey and Linton, 1981
	S($2p_{3/2}$)[b]	S^{2-}	161.3	67.33	Thomas et al., 1998
		S_2^{2-}	162.4	32.67	Thomas et al., 1998

[a] The binding energies are correct within ±0.2 eV.
[b] The S(2p) spectra was fitted using the doublets of S($2p_{3/2}$) and S($2p_{1/2}$) separated by 1.2 eV with their peak area ratio being 2:1. Although only the S($2p_{3/2}$) peak position was indicated, the area for S(2p) included those for S($2p_{3/2}$) and S($2p_{1/2}$).

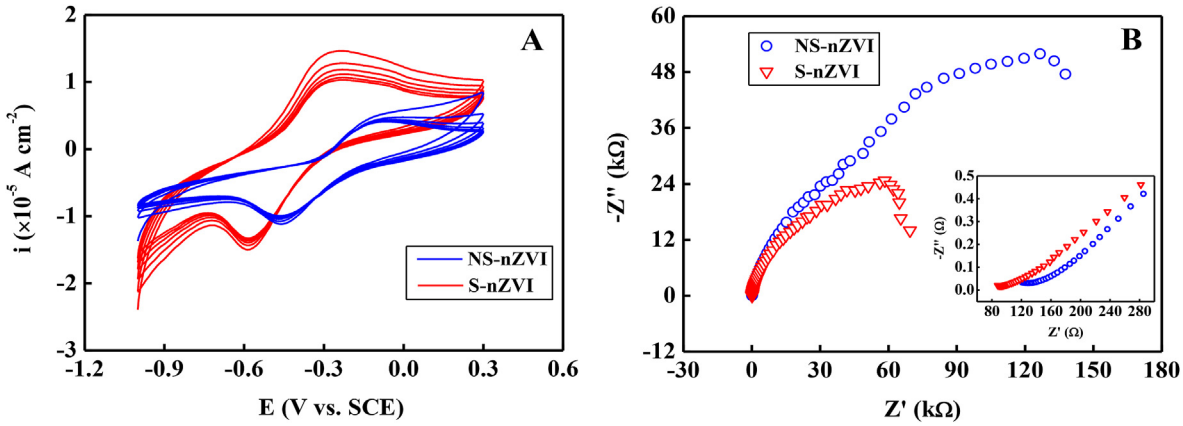

Fig. 2. The CV cycle profiles (A) and typical Nyquist plots (B) of the GCEs modified with S-nZVI and NS-nZVI. The inset in B showed details on results at low frequency.

step sequential pseudo-first-order rate model (Text S5 and Fig. S6). This discrepancy in the rates of TBBPA transformation between the NS-nZVI and S-nZVI system may be due to the formation of FeS on the nZVI surface. Lin et al. (2012) have reported that FeS could efficiently inhibit iron oxidation and corrosion of the nZVI, which could otherwise have led to a gradual loss of the reactive sites on nZVI for TBBPA as the reaction proceeded. In addition, the transformation rates of less brominated products (including tri-BBPA, di-BBPA and mono-BBPA) were also well described by the pseudo-first-order kinetic model (Text S5 and Fig. S6). The transformation rate constants of tri-BBPA, di-BBPA and mono-BBPA were 0.349 ± 0.007, 0.072 ± 0.005, 0.052 ± 0.004 h^{-1}, respectively. This fitting exercise strongly supported that the transformation of TBBPA by S-nZVI may follow a four-step sequential debromination pathway to form tri-BBPA, di-BBPA, mono-BBPA and BPA. It did not support a concerted debromination pathway from TBBPA to tri-BBPA, di-BBPA, mono-BBPA and to BPA in the S-nZVI system.

3.4. Aging effects of S-nZVI and NS-nZVI

Aging is generally thought to be associated with the formation of oxide film on the surface of nZVI, which can mask the redox active sites and thereby cause a dramatic reduction in the reactivity of nZVI with target contaminants (Guan et al., 2015). The NS-nZVI synthesized in our study was found little or no reactivity with TBBPA after 2 weeks of aging (Fig. 4A). Similar but less severe aging effects were reported in several previous studies. Sarathy et al. (2008) revealed that the 30-day old NS-nZVI could maintain approximately 30% of its original capacity of degrading carbon tetrachloride whereas Su et al. (2015) observed that the 3-week old NS-nZVI even maintained up to 70% of its original ability to remove cadmium. By contrast, our results showed that the S-nZVI was able to transform 55.5% of the initial TBBPA even after 11 weeks of aging (Fig. 4A). To our knowledge, 11 weeks is the longest aging time for S-nZVI reported in the literature. It has been suggested that sulfidation is beneficial for sustaining a reducing environment and decreasing the aggregation tendency of nZVI particles (Kim et al., 2014; Su et al., 2015), which were likely responsible for the enhanced longevity of S-nZVI in TBBPA transformation.

3.5. The reusability of S-nZVI and NS-nZVI

It is no doubt that reusability is one of the most important factors determining the applicability of nZVI-based nanoparticles in removal of target contaminants. However, little is done for evaluating the reusability of both traditional NS-nZVI for TBBPA transformation and S-nZVI for treating any target contaminants. As seen from Fig. 4B, the efficiency for TBBPA transformation by NS-nZVI decreased rapidly from 55%, to 25% and to 0% as the solid was used in the first, second and fourth cycle, respectively. Similar findings were also reported for NS-nZVI materials in reaction with other contaminants. For example, Xie et al. (2014) showed the

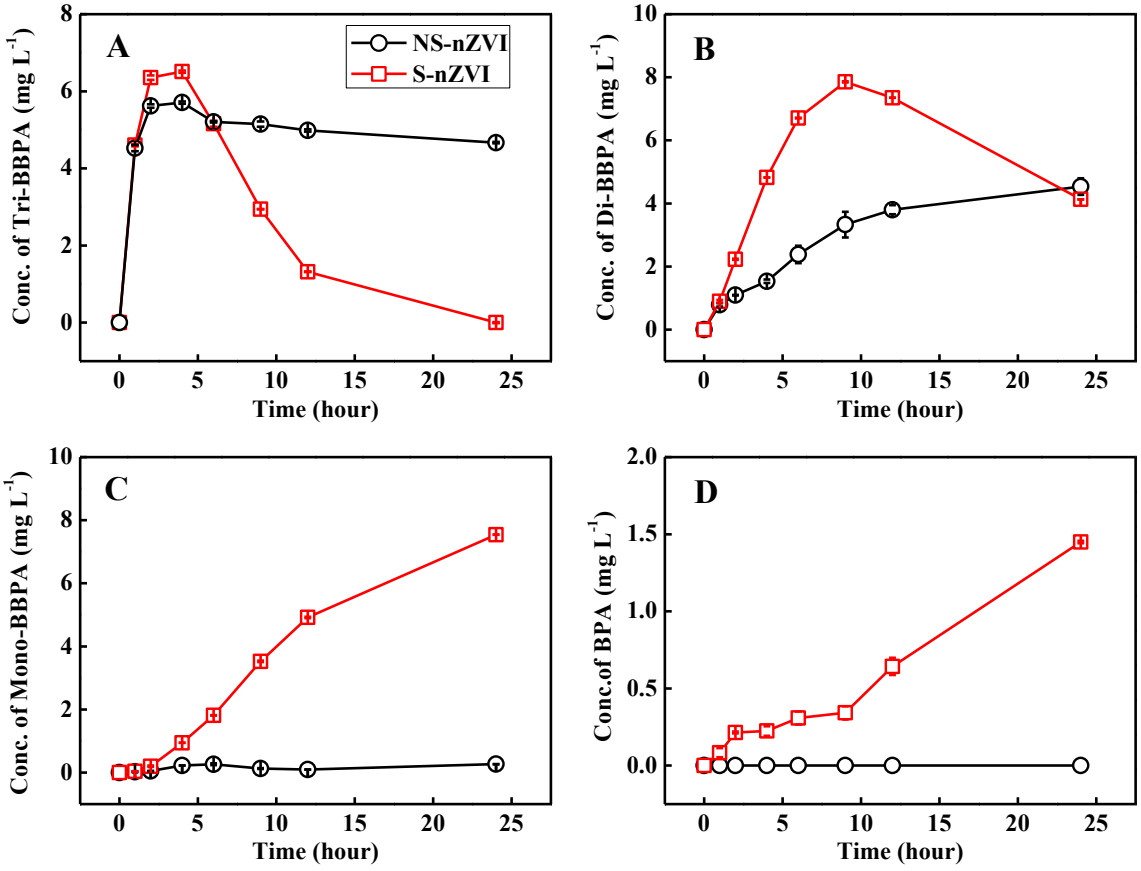

Fig. 3. The dynamics of the four products of TBBPA transformation by S-nZVI and NS-nZVI within 24 h of reaction.

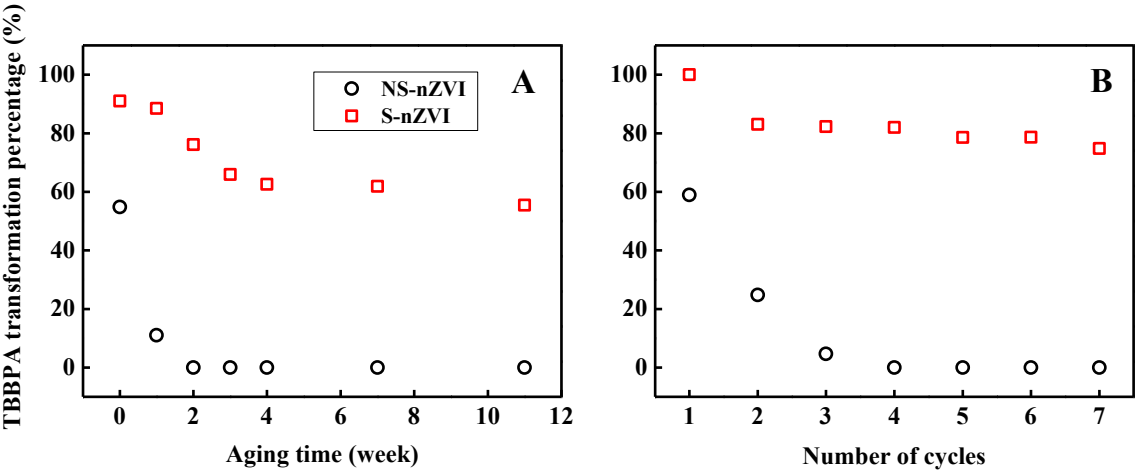

Fig. 4. The effects of aging (A) and reuse cycle (B) on the TBBPA transformation efficiencies of S-nZVI and NS-nZVI.

deca-BDE removal efficiency of NS-nZVI decreased from approximately 50% in the first cycle to 7.65% in the sixth cycle. They attributed the reduction of removal efficiency to the declining of specific surface area and dispersibility of NS-nZVI as particle agglomeration tended to increase with reuse cycle. By contrast, S-nZVI showed much higher reusability for TBBPA transformation as it maintained up to 80% of its original TBBPA transformation capacity even after 7 reuse cycles (Fig. 4B). Kim et al. (2011) revealed that the sulfidation could prevent agglomeration of the NS-nZVI particles, hence improving reusability of S-nZVI observed in this study. It is worth noting that several types of nZVI-based bimetallic nanoparticles also exhibited very high reusability for treating various halogenated organic pollutants. For instance, nano Ni/Fe was found to maintain approximately 90% and 70% of its original capacity for degrading deca-BDE in the seventh and eighth reuse cycles, respectively (Xie et al., 2014). However, the costs of synthesizing such bimetallic catalysts are far more expensive than that for S-nZVI.

3.6. Effect of S/Fe ratio

During synthesis of S-nZVI, the molar ratio of S/Fe in initial solution phase determines the sulfidation extent of the solid and thereby may control the efficiency of contaminant removal by the S-nZVI (Kim et al., 2011; Su et al., 2015). To evaluate such effects, three types of S-nZVI particles synthesized at three different S/Fe ratios (i.e., 0.12, 0.24 and 0.51) were evaluated for the rates of TBBPA transformation under the same reaction conditions. As shown in Fig. 5A, the rates of TBBPA transformation increased with the increasing S/Fe ratio. The rate constant (0.315 h^{-1}) calculated for the S-nZVI with the highest S/Fe ratio (0.51) was approximately 6.6 times greater than that for the solid having the lowest S/Fe ratio (0.12). In addition, the concentration of the final debrominated product (i.e., BPA) also increased with the increasing S/Fe ratio (Fig. 6A). The results suggested that higher sulfidation extent of

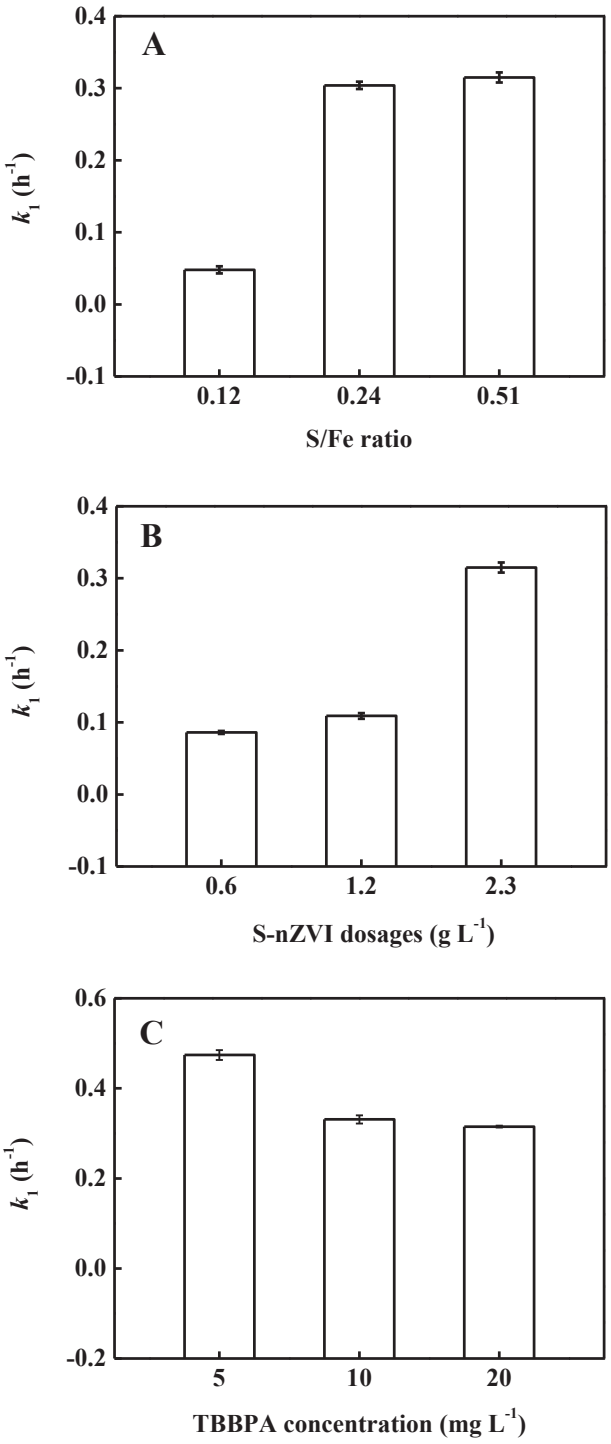

Fig. 5. The effects of S/Fe molar ratio (A), dosage of S-nZVI (B) and initial TBBPA concentration (C) on the transformation rate constant of TBBPA for S-nZVI.

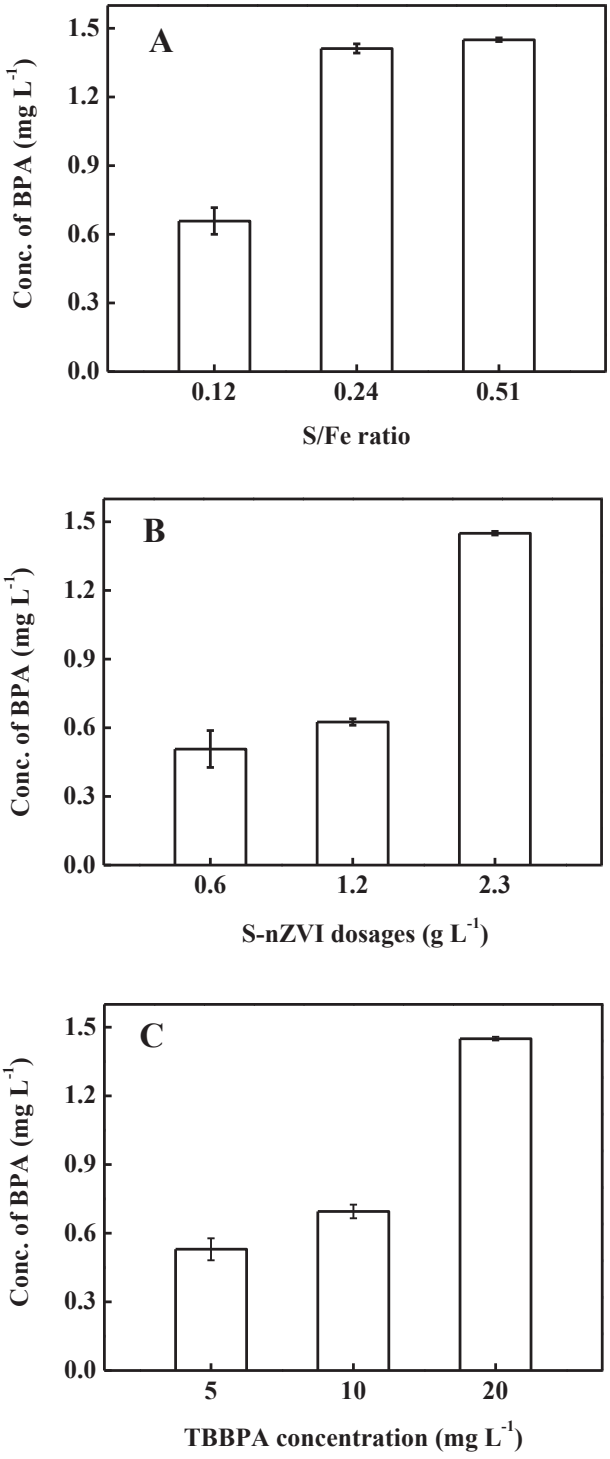

Fig. 6. The effects of S/Fe molar ratio (A), dosage of S-nZVI (B) and initial TBBPA concentration (C) on the level of BPA produced after 24 h of reaction between TBBPA and S-nZVI.

nZVI may favor faster transformation of TBBPA, which might be partly attributed to the increased specific surface area coupled with the increased S/Fe ratio (Table S1; Kim et al., 2011). However, Kim et al. (2011) reported that excessive sulfidation of nZVI likely led to redundant FeS deposition on its surface, which could block active sites and lower the rate of pollutant transformation. Further research is needed to optimize the S/Fe ratio for S-nZVI to achieve maximal TBBPA transformation capacity.

3.7. Effect of initial concentration of S-nZVI

The dosage of S-nZVI used in previous studies to react with target contaminants varied greatly from 0.6 to 35 g L^{-1} (Kim et al., 2011, 2013; Rajajayavel and Ghoshal, 2015; Su et al., 2015). Yet, the potential effect of S-nZVI dosage on the contaminant removal efficiency of S-nZVI remained unclear. In this study, we used three different S-nZVI (S/Fe ratio of 0.51) dosages (0.6, 1.2 and 2.3 g L^{-1}) for quantifying the rates of TBBPA transformation. The results showed that the transformation rate constant increased as a function of the S-nZVI dosage and that the rate constant obtained for the highest dosage was approximately 3.7 times greater than that for the lowest dosage (Fig. 5B). Meanwhile, the concentration of the final product BPA increased accordingly with the increased S-nZVI dosage as the BPA concentration was nearly 3 times greater in the highest dosage system than in the lowest one (Fig. 6B). Such results may be attributed proportionally to the increased reactive sites on more available surface area resulting from higher S-nZVI dosage. However, the relationship between S-nZVI dosage and its TBBPA transformation efficiency may be unimodal because excessive S-nZVI could increase the aggregation tendency of the nanoparticles and thereby decrease its reactivity as observed for NS-nZVI (O'Carroll et al., 2013).

3.8. Effect of initial TBBPA concentration

Transformation of TBBPA by nZVI-based nanoparticles involves heterogeneous reactions in which TBBPA molecules are adsorbed to the surface of the nanoparticles and subsequently undergo reductive transformation (Luo et al., 2010; Lin et al., 2012; Li et al., 2016a). The TBBPA transformation efficiency should remain at high levels when the starting TBBPA concentration increases initially, then decreases (or levels off) when the TBBPA molecules become excessive for the available reactive sites. To evaluate the effect of initial TBBPA concentration, a separate test using a fixed dosage (2.3 g L^{-1}) of S-nZVI (S/Fe ratio of 0.51) and three levels of initial TBBPA concentration (i.e., 5, 10 and 20 mg L^{-1}) was initiated. The results showed that the rate constant of TBBPA transformation decreased slightly from 0.474 to 0.315 h^{-1} when the initial TBBPA concentration increased from 5 to 20 mg L^{-1} (Fig. 5C), suggesting that 10 and 20 mg L^{-1} of TBBPA may be excessive for the available reactive sites at the tested conditions. Lin et al. (2012) reported that the rate constant of TBBPA transformation by NS-nZVI (3 g L^{-1}) decreased gradually when the initial TBBPA concentration increased from 1.0 to 8.0 mg L^{-1} and Li et al. (2016a) observed that the rate constant of TBBPA transformation by Ni/nZVI bimetallic nanoparticles (2 g L^{-1}) decreased linearly with the increasing initial TBBPA concentration ranging from 5 to 30 mg L^{-1}. In addition, Fig. 6C shows that the conversion percentage from TBBPA to BPA decreased from 23.2 to 15.3% as the initial TBBPA concentration increased, but the absolute BPA concentration increased considerably. The decrease conversion percentage indicated that excessive TBBPA added to the reaction system lowered the extent of debromination of TBBPA by the S-nZVI nanoparticles, which deserves future investigation.

3.9. Evaluation of cost-effectiveness

This study demonstrated that, compared to NS-nZVI, S-nZVI had much higher capacity and better performance for transforming TBBPA under the same experimental conditions, which renders lower cost in practical implementation of the S-nZVI technology. According to the cost analysis detailed in the Supporting Information (see Text S6), the cost for producing 1 kg of S-nZVI at S/Fe ratio of 0.51 is approximately 1.1 time as high as that for producing 1 kg of NS-nZVI. However the amount of the S-nZVI required for treating 1000 L of water containing 20 mg L^{-1} of TBBPA is less than 30% of that for NS-nZVI. Therefore, S-nZVI is likely much more cost effective than NS-nZVI in treating TBBPA polluted wastewater.

4. Conclusions

In this study, the reactivity of S-nZVI with TBBPA was quantified and compared with that of NS-nZVI. Our results showed that S-nZVI could transform over 90% of the initial TBBPA (20 mg L^{-1}) within 24 h of reaction, compared much favorably to the reaction efficiency of 55% by NS-nZVI. The rates of TBBPA transformation by S-nZVI and NS-nZVI followed respectively a pseudo-first-order rate model and a three-parameter single exponential decay model. S-nZVI was found capable of reductively transforming TBBPA into BPA at much faster rates than NS-nZVI, but both reaction systems may follow similar sequential pathway during transformation of TBBPA. Moreover, S-nZVI had much better longevity and reusability for TBBPA transformation than NS-nZVI. Results of XPS and electrochemical analyses suggested that the superior performances of S-nZVI on TBBPA transformation may be attributed largely to both the formation of an FeS layer on its surface and the elevated capacity for electron transfer by S-nZVI. The S/Fe molar ratio and dosage of S-nZVI as well as the initial TBBPA concentration could considerably affect the overall rate and extent of TBBPA transformation by S-nZVI. This study demonstrated that sulfidated nZVI can be considered as a promising alternative to the traditional NS-nZVI for remediation of aquatic environments contaminated with TBBPA.

Acknowledgments

This study was supported financially by the National Natural Science Foundation of China (Nos. 41120134006, 41173111 and 41473107). This is contribution No. IS-2266 from GIGCAS.

Appendix A. Supplementary data

Supplementary data related to this article can be found at http://dx.doi.org/10.1016/j.watres.2016.07.003.

References

Alaee, M., Arias, P., Sjödin, A., Bergman, Å., 2003. An overview of commercially used brominated flame retardants, their applications, their use patterns in different countries/regions and possible modes of release. Environ. Int. 29 (6), 683–689.
Bae, S., Gim, S., Kim, H., Hanna, K., 2016. Effect of $NaBH_4$ on properties of nanoscale zero-valent iron and its catalytic activity for reduction of *p*-nitrophenol. Appl. Catal. B Environ. 182, 541–549.
Chang, B.V., Yuan, S.Y., Ren, Y.L., 2012. Aerobic degradation of tetrabromobisphenol-A by microbes in river sediment. Chemosphere 87 (5), 535–541.
Covaci, A., Voorspoels, S., Abdallah, M.A.-E., Geens, T., Harrad, S., Law, R.J., 2009. Analytical and environmental aspects of the flame retardant tetrabromobisphenol-A and its derivatives. J. Chromatogr. A 1216 (3), 346–363.
Darnerud, P.O., 2003. Toxic effects of brominated flame retardants in man and in wildlife. Environ. Int. 29 (6), 841–853.
Decherf, S., Seugnet, I., Fini, J.-B., Clerget-Froidevaux, M.-S., Demeneix, B.A., 2010. Disruption of thyroid hormone-dependent hypothalamic set-points by environmental contaminants. Mol. Cell. Endocrinol. 323 (2), 172–182.
Guan, X., Sun, Y., Qin, H., Li, J., Lo, I.M.C., He, D., Dong, H., 2015. The limitations of applying zero-valent iron technology in contaminants sequestration and the

corresponding countermeasures: the development in zero-valent iron technology in the last two decades (1994-2014). Water Res. 75, 224–248.
Harrad, S., Abdallah, M.A.-E., Rose, N.L., Turner, S.D., Davidson, T.A., 2009. Current-use brominated flame retardants in water, sediment, and fish from English lakes. Environ. Sci. Technol. 43 (24), 9077–9083.
Harvey, D.T., Linton, R.W., 1981. Chemical characterization of hydrous ferric oxides by x-ray photoelectron spectroscopy. Anal. Chem. 53 (11), 1684–1688.
He, M.-J., Luo, X.-J., Yu, L.-H., Wu, J.-P., Chen, S.-J., Mai, B.-X., 2013. Diasteroisomer and enantiomer-specific profiles of hexabromocyclododecane and tetrabromobisphenol A in an aquatic environment in a highly industrialized area, South China: vertical profile, phase partition, and bioaccumulation. Environ. Pollut. 179, 105–110.
Huang, Q., Liu, W., Peng, P.A., Huang, W., 2013. Reductive debromination of tetrabromobisphenol A by Pd/Fe bimetallic catalysts. Chemosphere 92 (10), 1321–1327.
Ince, N.H., Tezcanli, G., Belen, R.K., Apikyan, İ.G., 2001. Ultrasound as a catalyzer of aqueous reaction systems: the state of the art and environmental applications. Appl. Catal. B Environ. 29 (3), 167–176.
Jeong, H.Y., Han, Y.-S., Park, S.W., Hayes, K.F., 2010. Aerobic oxidation of mackinawite (FeS) and its environmental implication for arsenic mobilization. Geochim. Cosmochim. Acta 74 (11), 3182–3198.
Kim, E.-J., Kim, J.-H., Azad, A.-M., Chang, Y.-S., 2011. Facile synthesis and characterization of Fe/FeS nanoparticles for environmental applications. ACS Appl. Mater. Interfaces 3 (5), 1457–1462.
Kim, E.-J., Kim, J.-H., Chang, Y.-S., Turcio-Ortega, D., Tratnyek, P.G., 2014. Effects of metal ions on the reactivity and corrosion electrochemistry of Fe/FeS nanoparticles. Environ. Sci. Technol. 48 (7), 4002–4011.
Kim, E.-J., Murugesan, K., Kim, J.-H., Tratnyek, P.G., Chang, Y.-S., 2013. Remediation of trichloroethylene by FeS-coated iron nanoparticles in simulated and real groundwater: effects of water chemistry. Ind. Eng. Chem. Res. 52 (27), 9343–9350.
Kitamura, S., Jinno, N., Ohta, S., Kuroki, H., Fujimoto, N., 2002. Thyroid hormonal activity of the flame retardants tetrabromobisphenol A and tetrachlorobisphenol A. Biochem. Biophys. Res. Commun. 293 (1), 554–559.
Levard, C., Hotze, E.M., Colman, B.P., Dale, A.L., Truong, L., Yang, X.Y., Bone, A.J., Brown, G.E., Tanguay, R.L., Di Giulio, R.T., Bernhardt, E.S., Meyer, J.N., Wiesner, M.R., Lowry, G.V., 2013. Sulfidation of silver nanoparticles: natural antidote to their toxicity. Environ. Sci. Technol. 47 (23), 13440–13448.
Li, D., Peng, P.A., Huang, W.L., Yu, Z.Q., Zhong, Y., 2016b. Reductive transformation of hexabromocyclododecane (HBCD) by FeS. Water Res. 101, 195–202.
Li, Y., Li, X., Xiao, Y., Wei, C., Han, D., Huang, W., 2016a. Catalytic debromination of tetrabromobisphenol A by Ni/nZVI bimetallic particles. Chem. Eng. J. 284, 1242–1250.
Lin, K., Ding, J., Huang, X., 2012. Debromination of tetrabromobisphenol A by nanoscale zerovalent iron: kinetics, influencing factors, and pathways. Indus. Eng. Chem. Res. 51 (25), 8378–8385.
Luo, S., Yang, S., Wang, X., Sun, C., 2010. Reductive degradation of tetrabromobisphenol A over iron-silver bimetallic nanoparticles under ultrasound radiation. Chemosphere 79 (6), 672–678.
Luo, S., Yang, S., Wang, X., Sun, C., 2011. Reductive degradation of tetrabromobisphenol using iron-silver and iron-nickel bimetallic nanoparticles with microwave energy. Environ. Eng. Sci. 29 (6), 453–460.
McCormick, J.M., Paiva, M.S., Häggblom, M.M., Cooper, K.R., White, L.A., 2010. Embryonic exposure to tetrabromobisphenol A and its metabolites, bisphenol A and tetrabromobisphenol A dimethyl ether disrupts normal zebrafish (*Danio rerio*) development and matrix metalloproteinase expression. Aquat. Toxicol. 100 (3), 255–262.
Morris, S., Allchin, C.R., Zegers, B.N., Haftka, J.J.H., Boon, J.P., Belpaire, C., Leonards, P.E.G., van Leeuwen, S.P.J., de Boer, J., 2004. Distribution and fate of HBCD and TBBPA brominated flame retardants in North Sea estuaries and aquatic food webs. Environ. Sci. Technol. 38 (21), 5497–5504.
Mukherjee, R., Kumar, R., Sinha, A., Lama, Y., Saha, A.K., 2016. A review on synthesis, characterization and applications of nano-zero valent iron (nZVI) for environmental remediation. Crit. Rev. Environ. Sci. Technol. 46 (5), 443–466.
Mullet, M., Boursiquot, S., Abdelmoula, M., Génin, J.-M., Ehrhardt, J.-J., 2002. Surface chemistry and structural properties of mackinawite prepared by reaction of sulfide ions with metallic iron. Geochim. Cosmochim. Acta 66 (5), 829–836.
O'Carroll, D., Sleep, B., Krol, M., Boparai, H., Kocur, C., 2013. Nanoscale zero valent iron and bimetallic particles for contaminated site remediation. Adv. Water Resour. 51, 104–122.
Osako, M., Kim, Y.-J., Sakai, S.-I., 2004. Leaching of brominated flame retardants in leachate from landfills in Japan. Chemosphere 57 (10), 1571–1579.
Pirlot, C., Deniau, G., Viel, P., Lécayon, G., Demortier, G., Delhalle, J., Mekhalif, Z., 2001. Study of the chemical transformations induced at the surface of bulk iron by protons and α beams. Nucl. Instrum. Methods Phys. Res. Sect. B Beam Interact. Mater. Atoms 185 (1–4), 71–76.
Rajajayavel, S.R.C., Ghoshal, S., 2015. Enhanced reductive dechlorination of trichloroethylene by sulfidated nanoscale zerovalent iron. Water Res. 78, 144–153.
Reinsch, B.C., Levard, C., Li, Z., Ma, R., Wise, A., Gregory, K.B., Brown, G.E., Lowry, G.V., 2012. Sulfidation of silver nanoparticles decreases *Escherichia coli* growth inhibition. Environ. Sci. Technol. 46 (13), 6992–7000.
Remya, N., Lin, J.-G., 2011. Current status of microwave application in wastewater treatment—a review. Chem. Eng. J. 166 (3), 797–813.
Rickard, D., 1995. Kinetics of FeS precipitation: part 1. Competing reaction mechanisms. Geochim. Cosmochim. Acta 59 (21), 4367–4379.
Sarathy, V., Tratnyek, P.G., Nurmi, J.T., Baer, D.R., Amonette, J.E., Chun, C.L., Penn, R.L., Reardon, E.J., 2008. Aging of iron nanoparticles in aqueous solution: effects on structure and reactivity. J. Phys. Chem. C 112 (7), 2286–2293.
Shahwan, T., Abu Sirriah, S., Nairat, M., Boyacı, E., Eroğlu, A.E., Scott, T.B., Hallam, K.R., 2011. Green synthesis of iron nanoparticles and their application as a Fenton-like catalyst for the degradation of aqueous cationic and anionic dyes. Chem. Eng. J. 172 (1), 258–266.
Su, Y., Adeleye, A.S., Keller, A.A., Huang, Y., Dai, C., Zhou, X., Zhang, Y., 2015. Magnetic sulfide-modified nanoscale zerovalent iron (S-nZVI) for dissolved metal ion removal. Water Res. 74, 47–57.
Thomas, J.E., Jones, C.F., Skinner, W.M., Smart, R.S., 1998. The role of surface sulfur species in the inhibition of pyrrhotite dissolution in acid conditions. Geochim. Cosmochim. Acta 62 (9), 1555–1565.
Turcio-Ortega, D., Fan, D., Tratnyek, P.G., Kim, E.-J., Chang, Y.-S., 2012. Reactivity of Fe/FeS nanoparticles: electrolyte composition effects on corrosion electrochemistry. Environ. Sci. Technol. 46 (22), 12484–12492.
Üzüm, Ç., Shahwan, T., Eroğlu, A.E., Lieberwirth, I., Scott, T.B., Hallam, K.R., 2008. Application of zero-valent iron nanoparticles for the removal of aqueous Co^{2+} ions under various experimental conditions. Chem. Eng. J. 144 (2), 213–220.
Vaughan, D.J., Ridout, M.S., 1971. Mössbauer studies of some sulphide minerals. J. Inorg. Nucl. Chem. 33 (3), 741–746.
Wang, J., Jia, X., Gao, S., Zeng, X., Li, H., Zhou, Z., Sheng, G., Yu, Z., 2016. Levels and distributions of polybrominated diphenyl ethers, hexabromocyclododecane, and tetrabromobisphenol A in sediments from Taihu Lake, China. Environ. Sci. Pollut. Res. 23 (11), 10361–10370.
Watson, J.H.P., Cressey, B.A., Roberts, A.P., Ellwood, D.C., Charnock, J.M., Soper, A.K., 2000. Structural and magnetic studies on heavy-metal-adsorbing iron sulphide nanoparticles produced by sulphate-reducing bacteria. J. Magn. Magn. Mater. 214 (1–2), 13–30.
Xie, Y., Fang, Z., Qiu, X., Tsang, E.P., Liang, B., 2014. Comparisons of the reactivity, reusability and stability of four different zero-valent iron-based nanoparticles. Chemosphere 108, 433–436.
Yan, M.-Y., Pang, Z.-H., Li, X.-M., Chen, J.-Y., Luo, J., 2013. Research on removal of tetrabromobisphenol A from synthetic wastewater by nanoscale zero valent iron supported on organobentonite. Environ. Sci. 34 (6), 2249–2255.
Yang, J., Chan, K.M., 2015. Evaluation of the toxic effects of brominated compounds (BDE-47, 99, 209, TBBPA) and bisphenol A (BPA) using a zebrafish liver cell line, ZFL. Aquat. Toxicol. 159, 138–147.
Zhang, K., Huang, J., Zhang, W., Yu, Y., Deng, S., Yu, G., 2012. Mechanochemical degradation of tetrabromobisphenol A: performance, products and pathway. J. Hazard. Mater. 243, 278–285.
Zheng, D., Ye, J., Zhou, L., Zhang, Y., Yu, C., 2009. Electrochemical properties of ordered mesoporous carbon film adsorbed onto a self-assembled alkanethiol monolayer on gold electrode. Electroanalysis 21 (2), 184–189.